In-situ monitoring of local bulk water contents and orientational order in paraffin/clay nanocomposites

Zbigniew Rozynek[1], René C Castberg[2], Alexander Mikkelsen[1] and Jon Otto Fossum[1,3]

[1] Department of Physics, NTNU, Høgskoleringen 5, NO-7491 Trondheim, Norway
[2] Physics Department, University of Oslo, Postboks 1048, NO-0316, Oslo, Norway
[3] Center for Advanced Study, Drammensvegen 78, NO- 0272, Oslo, Norway

E-mails: zbigniew.rozynek@ntnu.no, jon.fossum@ntnu.no

Abstract

We study the behaviour of fluorohectorite synthetic clay particles dispersed in paraffin-wax. First, we report wide angle X-ray scattering related to electric-field-induced alignment of the embedded clay particles. Secondly, we provide observations of system anisotropy during melting and crystallization of clay/paraffin nanocomposites. Finally, the time evolution of the one-to-zero/zero-to-one water layer transition in paraffin embedded fluorohectorite clay galleries is presented, and we demonstrate that such particles can be used as 'meso-detectors' for monitoring the local water content in bulk carrier matrices, such as paraffin-wax.

Keywords: composite, diffusion, XRD

1. Introduction

Clay particles have the ability to change and improve many physical properties, e.g. mechanical strength, thermal stability, conductivity, etc. of the medium in which they are suspended [1,2,3]. Some of these properties can be anisotropically enhanced if the particles are orientationally aligned in the host medium. Such a particle organization can be utilized as a molecular barrier, i.e. the permeability of gas molecules in polymer/clay composites are significantly reduced in the direction normal to clay platelet surfaces, whereas no change is expected for molecules propagating along the oriented clay surfaces. Yano et al. [4] report that only a 2 wt.% addition of montmorillonite clay particles into polyimide may lower the gas permeability down to a value less than half of the pure polyimide gas permeability. Alignment of clay particles can be induced by planar shearing [5], extrusion [6], gravity [7], and magnetic [8] or electric fields [9].

An electric field is often used to produce anisotropic structures in order to obtain desirable physical properties. When polarizable particles are exposed to an *E*-field of either alternating-current (AC) or direct-current (DC), dipoles will be induced and result in a rotational force on the particles in accordance with the Clausius–Mossotti relation [10]. The particle alignment can be monitored by means of X-ray or neutron diffraction [11,12], and the degree of anisotropy can be quantified and expressed in terms of an order parameter S_2 [7,13] (for details see Section 3.3).

In previous studies by our group, the average orientational clay distribution was measured in a silicone oil system [9,11]. In the present study the clay particles are instead dispersed in melted paraffin-wax. There are some important differences between this system and the silicone oil system: The paraffin-wax viscosity is significantly higher, since the paraffin molecules are longer than the oil molecules, and thus clay alignment is achieved at higher temperatures, i.e. between 65 and 100 ºC, and is slower than for the silicon oil case. Therefore in the present case of paraffin-wax, we are able to monitor the increase of orientational order dynamically.

We are here also concerned with studying the amount of water that is intercalated inside clay galleries. It is well-known that the swelling/shrinking of layered clay particles consists of changes in the interlayer repetition distance (*d*-spacing), and these changes can be monitored by means of X-ray diffraction. The amount of intercalated water is a function of temperature and relative humidity (RH) of the clay surroundings. Hemmen et al. [14,15] showed that by measuring the interlayer repetition distance *d* it is possible to (i) estimate a local humidity surrounding the clay particles, and thus (ii) monitor quasi one-dimensional diffusion of water through the bulk sample, and finally (iii) extract profiles of RH along the sample. Here, we wish to investigate the time-dependent changes in the intercalated water content of clays in both the melted state and in the crystalized paraffin. This is the initial step for further measurements of anisotropic water diffusion through paraffin matrices with aligned clay particles.

The layout of this article is as follows: First, the sample preparation and the experimental procedures are explained in section 2. Wide angle X-ray scattering results are presented in section 0,

including: alignment of clay particles in *E*-field (section 3.1); the development of the system anisotropy during melting and crystallization (section 3.2); time dependent one-to-zero water layer transition (section 3.3); and finally zero-to-one water layer transition (section 3.4). Conclusions and suggestions for further work are presented in the final section, 4.

2. Sample description, preparation, and experimental procedures

2.1. Li-Fh clay particles

In this work we have chosen to work with the synthetic clay fluorohectorite. There are several reasons for this choice. Firstly, in terms of structure, fluorohectorite is virtually identical to natural smectite clays such as montmorrillonite **[16]**. Secondly, our group has studied fluorohectorite as a model system for clays **[17,18,19]** for many years and this system is thus understood and characterized in detail.

Lithium fluorohectorite (Li-Fh) was purchased from Corning Inc., New York in the form of a white powder. Li-Fh is a synthetic 2:1 smectite clay having the nominal chemical formula $Li^{+}_{1.2}[Mg_{4.8}Li_{1.2}Si_8O_{20}F_4]^{-1.2}$ per unit cell, where Li^{+} is an interlayer exchangeable cation. Li-Fh has a surface charge of 1.2 e^{-}/unit cell and is a polydisperse clay with platelet diameters ranging from a few hundred nm up to a few μm **[18]**. A *single* particle consists of about 80–100 platelets (crystalline sheets) **[14,15]** that stack on top of one another forming a "deck of cards" structure. Since the thickness of such a stack is approximately 0.1 μm, the resulting particle has a diameter-to-height ratio on average close to 20:1 on average. However, the *single* particles tend to agglomerate when dispersed into a non-polar medium (oils, polymeric matrices, etc.), unless chemically modified **[20]**. Both the shape and size of aggregated structures may vary, and in general they depend on clay type and sample preparation **[21,22,23]**. The Li-Fh clay absorbs water, which makes it swell. The swelling of layered 2:1 smectite clay particles is caused by a change in the interlayer repetition distance between crystalline sheets (*d*-spacing) **[24]**.

2.2. Paraffin-wax

Paraffin-wax normally refers to a mixture of *n*-alkanes (chemical formula C_nH_{2n+2}) with *n* ranging between 20 and 40 determining the characteristic length of the molecules and also the melting temperature of the paraffin matrix. The material used for the present composite preparation was ordered from Sigma-Aldrich (ASTM D 127, batch: MKBC6750). This particular type of paraffin wax has its melting point around 65 ºC and was chosen due to the following reasons: (i) the X-ray peak positions related to the characteristic molecule dimensions should not overlap with clay reflections related to the interlamellar distance; (ii) optimal melting and crystallization temperatures providing both the ease of composite preparation and appropriate stiffness of the composite when in solid form at room temperature; (iii) relatively non-polar and non-conductive material that can be used as an electrorheological carrier fluid for clay particles when in the melted state.

The characterization of the pure paraffin-wax by means of X-ray scattering and rheometry is presented in the supporting materials (see Figure S1 and Figure S2).

2.3. Preparation of paraffin/clay composites

The first sample batch was prepared to monitor the dynamic alignment of clay particles during the composite melting and crystallization inside a custom-made heating cell. The sample batch was made as follows: 1.4 g of Li-Fh clay powder was slowly added into 7 g of pre-melted paraffin-wax. After 10 min of stirring, the solution was left to rest for 3 min in order to allow the biggest clay particles to sediment. The top part (80 % of the solution), consisting of the smallest clay particles, was then poured into a 10 ml glass phial. The solution was kept at a temperature between 80-90 °C and stirred for 1h in order to disperse clay particles within the paraffin. The solution was then cooled down, and the solid cast was cut into small pieces that could fit inside the sample holder of the heating cell (see Figure S3 in supporting material).

The second sample batch was prepared for in-situ monitoring of water content in clays embedded in paraffin matrix. The composites were made as follows: 1.4 g of Li-Fh clay powder was slowly

added into 7 g of pre-melted paraffin wax. After 10 min of stirring, the solution was left to rest for 3 min in order to allow the biggest clay particles to sediment. The top part (80 % of the solution), consisting of the smallest clay particles, was then poured into a 10 ml glass phial. The solution was stabilized at a temperature around 120-130 °C while stirring. The temperature was higher for this batch compared to the first sample batch, since we wish to monitor the time-dependent dehydration in clays, i.e. the one-to-zero water transition. Every hour, around 0.5 ml of solution was taken out to make a solid cast and X-rayed immediately after each composite had solidified. The same samples (stored in a solid form at room temperature and relative humidity between 45 and 55 %) were re-examined by X-ray scattering 6 months later in order to monitor changes in the water content. The dimensions of composites are 30 x 6.5 x 1.5 mm^3. An example of a solid cast is shown in supporting Figure S4. In all samples the clay concentration was estimated to be around 5 % by weight.

2.4. Wide-angle X-ray scattering experimental procedures

Investigations of the dynamic alignment of clay particles (sample batch 1) were performed at the European Synchrotron Radiation Facility (ESRF) in Grenoble, France. An X-ray beam with a wavelength of 0.9Å and a 0.3x0.3 mm^2 beam size at the sample was used. The beamline BM01A is equipped with a two-dimensional MAR345 image plate detector with a diameter of 345 mm. The available scattering q-range is 0.03 – 1.6 Å. The custom-made sample cell from NTNU (Figure S3) enabled precise control of heating and cooling in temperature range between 20 – 100 °C.

The second sample batch was investigated at our home laboratory (NTNU, Trondheim, Norway) using NanoSTAR from Bruker AXS setup in a wide-angle X-ray scattering (WAXS) mode. The instrument is equipped with a CuKα Xenocs micro-source that emitts X-rays at wavelength 1.5418 Å. and a 2-D gas detector that collects Bragg diffraction rings allowing investigations of the orientational distribution of the clay platelet stacks embedded in the paraffin-wax matrix. The beam size at the sample is about 0.4 mm in diameter and the available scattering q-range for the setup is 0.08 – 1 $Å^{-1}$. The sample-to-detector distance was calibrated using a silver behenate standard.

3. Results

3.1. Electric-field-induced alignment of clay particles

Figure 1 shows two examples of the two-dimensional WAXS patterns from paraffin/clay composites without (left) and with (right) an external electric field applied. The outermost ring originates from the Bragg 001 reflection that corresponds to the distance between clay's crystalline layers. It becomes anisotropic in the presence of an *E*-field due to clay particle alignment.

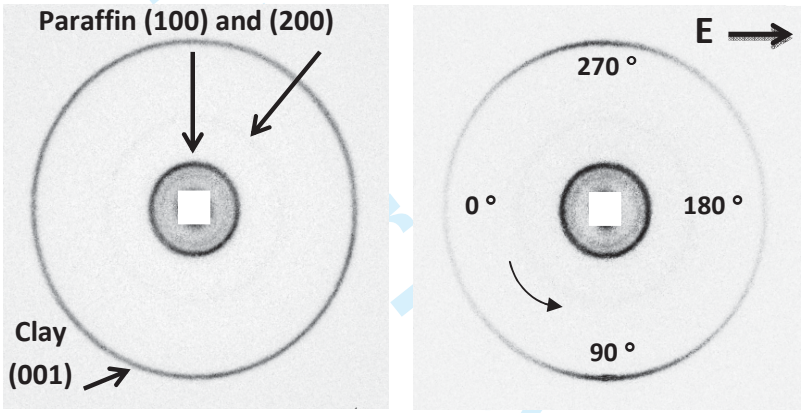

Figure 1. Two-dimensional WAXS patterns from paraffin/clay composites without (left) and with (right) an external *E*-field of 250 V/mm applied. The outermost ring from clay becomes anisotropic indicating that clay particles are aligned with their stacking direction perpendicular to the *E*-field lines.

To quantify the degree of anisotropy of the system, i.e. how well the clay platelets align with respect to the *E*-field direction, one needs to integrate the 2-D WAXS patterns (corresponding to the width of the 001 clay peak) radially over a narrow *q*-range and fit the obtained azimuthal plot (see Figure 3) to a parametric function. The Maier-Saupe function can be used for such a parametric fit (for details see **[11,13,25]**). In short, the fitting parameter is a measure of the peak full width at half maximum, i.e. a smaller value equals a higher degree of anisotropy, and can be expressed as the nematic order parameter S_2. The values of this parameter ranges from -1/2 to 1, where 1 indicates perfectly oriented platelet particles in the nematic configuration, 0 states no orientational order, and -1/2 indicates perfectly oriented pplatelets in the so-called anti-nematic configuration **[11,13,25]**.

We are expecting the clay particles to align in the anti-nematic fashion when an external *E*-field is applied **[11,13]**. The validity of such an assumption is tested here by investigation of the clay particle alignment as a function of the polar angle. Ninety two-dimensional WAXS images of the solidified sample were captured at different polar angles with the rotation axis parallel to the *E*-field direction. The nematic order parameters were calculated for each sample position. The results are presented in Figure 2 where S_2 values are plotted against the rotation angle. One sees that the nematic order parameter values do not differ significantly from each other, indicating that there is no preferential orientation along the polar angle, as represented by the arrowed disc shown in the inset of Figure 2 which represents the plane normal to the *E*-field direction. Thus we can be confident that the anti-nematic configuration applies for the clay particles in the present case.

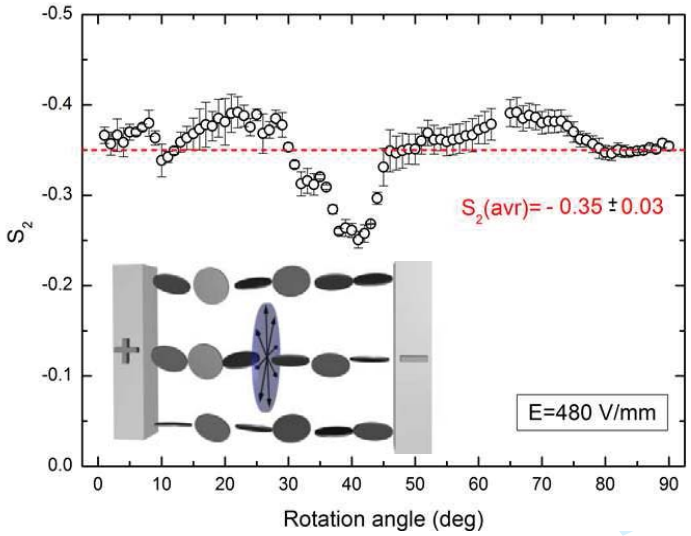

Figure 2. The nematic order parameter calculated for different rotation angles. The average S_2 value is indicated as a dashed line. The inset shows a sketch of the clay alignment in a so-called anti-nematic configuration (see text for details).

To examine whether the alignment of clay particles may be disrupted during paraffin crystallization, the nanoparticles' dispersion state was monitored during heating and cooling using the custom made sample cell. X-ray diffractograms were first collected for samples at room temperature with no preferential orientation. Electric field (250 V/mm, 100 Hz, square wave) was applied from the beginning of the measurements, and it did not affect the samples while in solid form. Figure 3 shows

1-D azimuthal plots (only 4 out of 64 measurements are shown for sake of clarity), where the 001 Bragg peak amplitudes (clay stacking) increase when paraffin melts and clay particles start aligning.

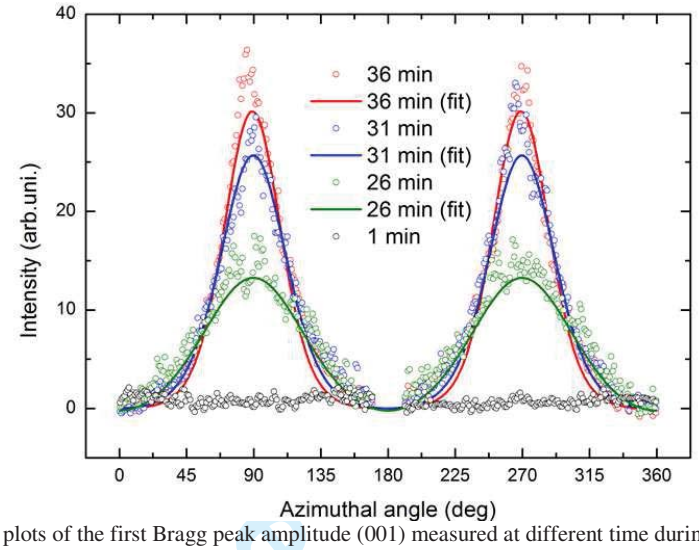

Figure 3. Azimuthal plots of the first Bragg peak amplitude (001) measured at different time during the paraffin melting.

The scattered points are the experimental data, whereas the lines are the Maier-Saupe fits. The results of fitting are presented in Figure 4. The nematic order parameter S_2=0 was ascribed by default for data points measured from 0-23 min, since it was impossible to converge the 1-D azimuthal plots with the fitting curve (as the black open circles in Figure 3).

The degree of anisotropy in the system increases when the paraffin starts melting and S_2 reaches a maximum value -0.36 at t=36 min. Interestingly, as time passes, the anisotropy starts decreasing slightly and the value of S_2 changes by ~15 %, and ut thus seems like a better particle alignment is achieved before individual particles start forming column-like structures. After 54 min, the sample was cooled down. It took around 5 min for paraffin to start crystalizing. A small drop in S_2 was observed during that time. This might be caused by the paraffin crystallization. The final measured nematic order parameter value (last minutes - solid sample) is -0.32. More measurements are needed in order to be more conclusive on these points.

Compared to particle alignment in clay/silicone oil-suspension (at room temperature) studied by our group previously, the characteristic rotation time τ_R (alignment of clay particles along the *E*-field lines) is longer in the present case, since the paraffin-wax is significantly more viscous than the

silicone oil used in previous work [11]. Recently, this rotation time has been shown to be proportional to E^2 and inversely proportional to the viscosity of the carrier fluid [26].

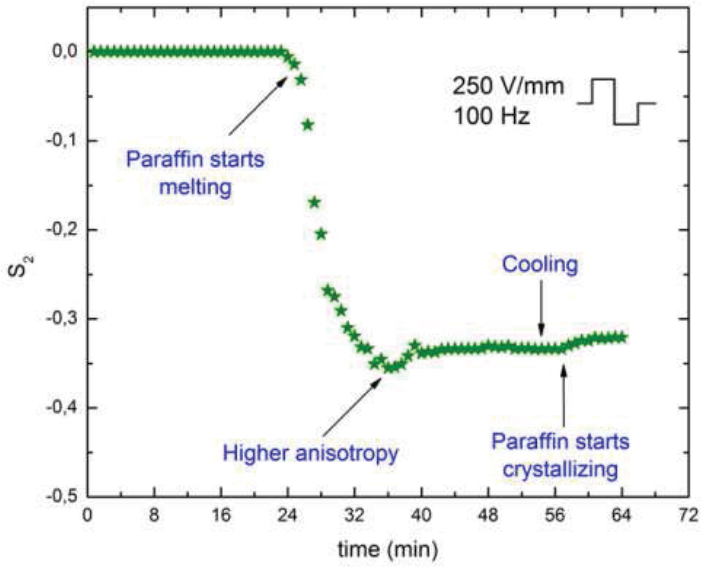

Figure 4. Development of the anisotropy in the system expressed by changes in the nematic order parameter S_2.

3.2. One-to-zero water layer transition

Water can intercalate in between each fluorohectorite platelet in the stack, causing the clay particle stack to swell. For Li-Fh, the intercalation process which is temperature and relative humidity dependent yields four stable hydration states [27]. The structures, referred to as having 0, 1, 1.5 or 2 intercalated water layers respectively, are quite well ordered along the stacking direction. The unit cell along the stacking direction is given by the distance between the stacked platelets, and the d-spacing in this direction is close to 1.0, 1.2, 1.35 and 1.5 nm for the case of 0WL, 1WL, 1.5WL and 2WL, respectively.

The samples from the second batch were measured to investigate the time-dependent changes in water content intercalated between the clay's crystalline sheets. The recorded X-ray data allow monitoring of the evolution of one-to-zero and zero-to-one water layer transitions.

Figure 4 shows azimuthally integrated two-dimensional WAXS patterns from six samples prepared at different times, namely for 0, 2, 3, 5, 7 and 10 h of stirring at elevated temperature around 120-130

°C. Initially, the clay particles (kept at room temperature and ambient humidity, in form of powder) were in the pure 1WL hydration state (first measurement - blue dotted curve). The corresponding 001 Bragg peak is located at 1.21 nm. After two hours, the 1WL-peak intensity decreased and a new, broad and not yet distinct peak appeared with a distance corresponding to the 0WL hydration state. The peaks are asymmetric with respect to their intensities and widths, and both peaks are shifted from their initial d_{100}^{1WL}=1.21 nm and final d_{100}^{0WL} =1.03 nm positions towards lower and higher values (d_{100}^{1WL} =1.19 nm and d_{100}^{0WL} =1.07 nm), respectively. The intensity of the peak related to 0WL state increases with time and becomes sharper. After 5 h, the population of clay particles in the scattering volume contains a significantly higher proportion of 0WL over 1WL spacings. The clay particles need almost 10 h to reach nearly pure 0WL hydration final state (red curve with triangles). A minor population of clay particles possessing the intercalated water is still present, but is hardly detectable by our instrument.

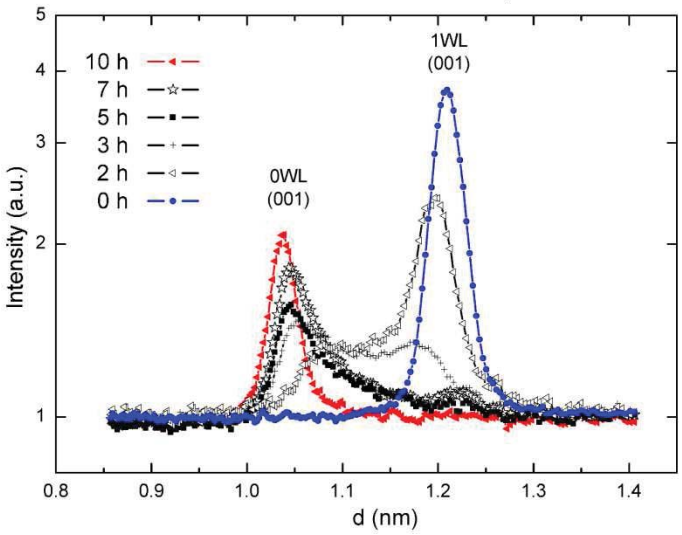

Figure 5. Time evolution of the 1-to-0 water layer transition (Sample batch 2).

The interlayer hydration states occurring in smectite clays are pure water layer states (i.e. 0WL, 1WL, (1.5WL) and 2WL) **[28]**, and in addition Hendricks-Teller mixed hydration states occur as reported by Michels et al. **[29].** Recently Hemmen et al. **[14,15]** thoroughly mapped systematic changes in the d-spacing values within the pure WL states as a function of relative humidity, and investigated the 1-to-2 WL transition. In the present case the 1-to-0 WL transition was monitored. The

maximum values of the smooth changes in the *d*-spacing, with respect to both the initial and the final state (1WL→0WL), are on the order of approximately 0.3 Å for deviation from 1WL, and 0.5 Å for deviation from 0WL. These values are similar to those that Hemmen et al. **[14,15]** reported.

3.3. Zero-to-one water layer transition

The same samples (kept in a solid form) were investigated 6 months later in order to monitor the water contents. The time 2:1 smectite clays require to hydrate depends on relative humidity (RH) and temperature together with the size and charge of the exchangeable cation in the interlayer space. For powdered samples the time evolution magnitude is on the order of hours **[30,31,32,33]**. However, the time needed for the entire clay population (inside the paraffin-wax) to reach the 1WL state is considerably longer. The effective RH around embedded clay particles is low, since the water penetration through the oligomer matrix is restrained.

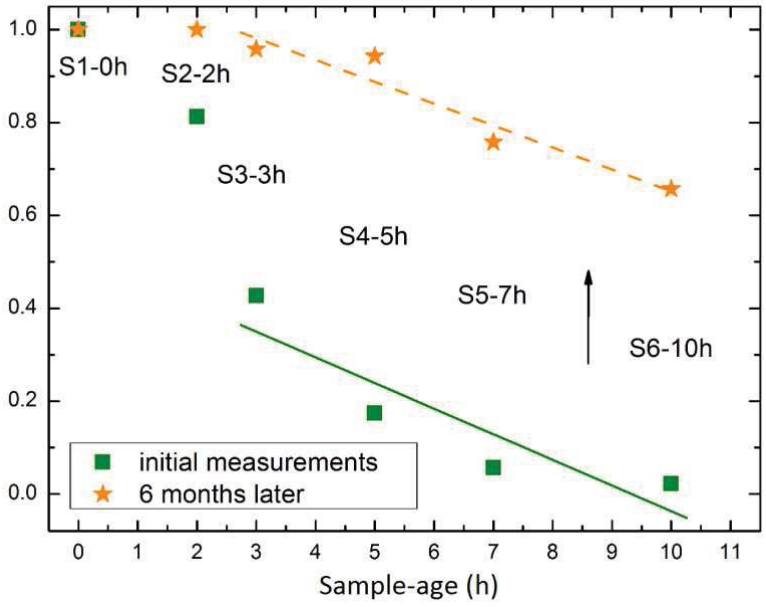

Figure 6. The ratios $I_1/(I_1+ I_2)$ between magnitudes of 0WL and 1 WL peak intensities for 6 samples (Sample batch 2). Their values are in range 0-1, where 0 indicates a pure dehydrated state, 0.5 is obtained when the number of clay particles in the two states are equal, whereas 1 depicts the pure mono-hydrated state.

Figure 6 shows $I_1/(I_1+I_2)$ magnitude ratios for 0WL and 1 WL peak intensities for 6 samples from the second sample batch. The ratio values are in range 0-1, where 0 indicates a pure dehydrated state, 0.5 is obtained when the number of clay particles in the two states is equal, and 1 depicts the pure

mono-hydrated state. Green squared data points were acquired from measuring samples right after their preparation (as shown also in Figure 5). Orange star data points were obtained from the same samples, measured 6 months later. For all samples (S1-0h omitted in this discussion), water molecules intercalate into the clay galleries. However, the complete recovery from a partially dehydrated state (0WL) to a mono-hydrated state (1WL) was only accomplished by the sample labelled S2-2h. By comparing the intensity ratio values, it can be concluded that the remaining four samples absorbed comparable amounts of water. The two lines in Figure 6 were obtained by fitting the data points to a linear function $y=a+bx$. The calculated values of the slope b were very similar for the two sets, i.e. -0.05±0.02 and -0.06±0.02 for the (dashed) orange and (solid) green curve, respectively.

4. Conclusions

We have investigated the electric field induced alignment of fluorohectorite clay particles in oligomeric matrices, and the development of the system anisotropy was observed during paraffin melting and crystallization. Interestingly, it was found that on average the clay particles loose some of their orientational order to accommodate chain formation.

The dehydration of clay particles as a function of time was also investigated, and our observations show that it takes almost 10 h for the clay particles in the melted wax to reach the pure 0WL hydration final state. However, the zero-to-one water layer transition for clay particles being embedded in crystalized paraffin is very slow. This is due to a very low water penetration through the oligomer matrix. Even after 6 months with air exposure, the sample still contains a population of clay particles possessing no or very little intercalated water. This suggests that such embedded clay particles can be used as ‘meso-detectors’ for monitoring the local water content in such bulk carrier matrices. We plan future work in this direction including investigations of possibly anisotropic water diffusion through paraffin matrices with aligned clay particles.

Acknowledgements

The authors would like to thank Kenneth Dahl Knudsen and Elisabeth Lindbo Hansen for their helpful comments on the manuscript, and also D. Chernyshov for his assistance while performing experiments at the Swiss-Norwegian Beam Lines at ESRF. Yves Méheust and Henrik Hemmen are acknowledged as creators of the script for fitting the data to the Maier-Saupe function. The 2-D WAXS diffractograms were analyzed using Fit2D created by A. P. Hammersley. This work was supported by the Research Council of Norway through the FRINAT Program: NFR project number 171300, the NANOMAT Program: NFR project number 182075 and the SYNKNØYT Program.

References

1. H. J. Walls, M. W. Riley, R. R. Singhal, R. J. Spontak, P. S. Fedkiw and S. A. Khan: Nanocomposite electrolytes with fumed silica and hectorite clay networks: passive versus active fillers. *Adv. Funct. Mater.* **13** 710-717 (2003).
2. S. H. Kim, J. Eun-Ju, Y. Jung, M. Han and S. J. Park: Ionic conductivity of polymeric nanocomposite electrolytes based on poly(ethylene oxide) and organo-clay materials. *Colloid. Surface.* **313** 216-219 (2008).
3. D. Ratna, S. Divekar, A. B. Samui, B. C. Chakraborty and A. K. Banthia: Poly(ethylene oxide)/clay nanocomposite: Thermomechanical properties and morphology. *Polymer* **47** 4068-4074 (2006).
4. K. Yano, A. Usuki, A. Okada, T. Kurauchi and O. Kamigaito: Synthesis and Properties of Polyimide-Clay Hybrid. *J. Polym. Sci. A* **31** 2493–2498 (1993).
5. M. Okamoto, P. H. Nam, P. Maiti, T. Kotaka, T. Nakayama, M. Takada, M. Ohshima, A. Usuki, N. Hasegawa and H. Okamoto: Biaxial Flow-Induced Alignment of Silicate Layers in Polypropylene/Clay Nanocomposite Foam. *Nano Lett*. **1** 503-505 (2011).
6. X. He, J. Yang, L. Zhu, B. Wang, G. Sun, P. Lv, I. Y. Phang and T. Liu: Morphology and Melt Rheology of Nylon 11/Clay Nanocomposites. *Appl. Polym. Sci*. **102** 542–549 (2006).
7. H. Hemmen, N. I. Ringdal, E. N. De Azevedo, M. Engelsberg, E. L. Hansen, Y. Méheust, J. O. Fossum and K. D. Knudsen: The Isotropic-Nematic Interface in Suspensions of Na-Fluorohectorite Synthetic Clay. *Langmuir* **25** 12507–12515 (2009).
8. E. N. De Azevedo, M. Engelsberg, J. O. Fossum and R. E. de Souza: Anisotropic Water Diffusion in Nematic Self-Assemblies of Clay Nanoplatelets Suspended in Water. *Langmuir* **23** 5100 (2007).
9. J. O. Fossum, Y. Méheust, K. P. S. Parmar, K. D. Knudsen, K. J. Måløy and D. M. Fonseca: Intercalation-enhanced electric polarization and chain formation of nano-layered particles. *Europhys.Lett.* **74** 438-444 (2006).
10. Y. P. Huang, M. J. Lee, M. K. Yang and C. W. Chen: Montmorillonite particle alignment and crystallization and ion-conducting behavior of montmorillonite/poly(ethylene oxide) nanocomposites. *Appl. Clay Sci.* **49** 163-169 (2010).
11. Z. Rozynek, K. D. Knudsen, J. O. Fossum, Y. Méheust, B. Wang and M. Zhou: Electric field induced structuring in clay–oil suspensions: new insights from WAXS, SEM, leak current, dielectric permittivity, and rheometry. *J. Phys.: Condens. Mat.* **22** 324104 (2010).
12. K. D. Knudsen, J. O. Fossum, G. Helgesen and M. W. Haakestad: Small-angle neutron scattering from a nano-layered synthetic silicate. *Physica B: Condens. Mat.* **352** 247 (2004).
13. Y. Méheust, K. D. Knudsen and J. O. Fossum: Inferring orientation distributions in anisotropic powders of nano-layered crystallites from a single two-dimensional WAXS image. *J. Appl. Cryst.* **39** 661-670 (2006).
14. H. Hemmen, L. R. Alme, J. O. Fossum and Y. Méheust: X-ray studies of interlayer water absorption and mesoporous water transport in a weakly hydrated clay. *Phys.Rev. E* **82** 036315 (2010).
15. H. Hemmen, L. R. Alme, J. O. Fossum and Y. Méheust: Erratum: X-ray studies of interlayer water absorption and mesoporous water transport in a weakly hydrated clay. *Phys.Rev. E* **83** 019901(E) (2011).

16. P. D. Kaviratna, T. J. Pinnavaia and P. A. Schroeder: Dielectric properties of smectite clays. *J. Phys. Chem. Solids* **57** 1897 (1996).
17. J. O. Fossum: Physical phenomena in clays. *Physica A* **270** 270 (1999).
18. J. O. Fossum: Flow of clays. *Eur. Phys. J. Special Topics* **204** 41-56 (2012).
19. E. L. Hansen, H. Hemmen, D. M. Fonseca, C. Coutant, K. D. Knudsen, T. S. Plivelic, D. Bonn and J. O. Fossum: Swelling transition of a clay induced by heating. *Scientific Reports* **2:**618 (2012).
20. B. Wang, M. Zhou, Z. Rozynek and J. O. Fossum: Electrorheological properties of organically modified nanolayered laponite: influence of intercalation, adsorption and wettability. *J. Mater. Chem.* **19** 1816-1828 (2009).
21. Z. Rozynek, T. Zacher, M. Janek, M. Čaplovičová and J. O. Fossum: *Electric-field-induced structuring and rheologicalproperties of kaolinite and halloysite clays,* **submitted** to Appl.Clay Sci.
22. Z. Rozynek, B. Wang, J. O. Fossum and K. D. Knudsen D: Dipolar structuring of organically modified fluorohectorite clay particles. *Eur. Phys. J. E* **35**:9 (2012).
23. Z. Rozynek, H. Mauroy, R. C. Castberg, K. D. Knudsen and J. O. Fossum: Dipolar ordering of clay particles in various carrier fluids. *Rev. Cub. Fis.* **29** 1E37 (2012).
24. G. J. Silva, J. O. Fossum, E. DiMasi, K. J. Måløy and S. B. Lutnæs: Synchrotron x-ray scattering studies of water intercalation in a layered synthetic silicate. *Phys.Rev. E* **66** 011303 (2002).
25. I. Dozov, E. Paineau, P. Davidson, K. Antonova, C. Baravian, I. Bihannic and L. J. Michot: Electric-Field-Induced Perfect Anti-Nematic Order in Isotropic Aqueous Suspensions of a Natural Beidellite Clay. *J. Phys. Chem. B* **115** 7751–7765 (2011).
26. R. C. Castberg, Z. Rozynek, J. O. Fossum, K. J. Måløy, P. Dommersnes and E. G. Flekkøy: 26. Clay alignment in electric fields. *Rev. Cub. Fis.* **29** 1E17 (2012).
27. R. P. Tenorio, M. Engelsberg, J. O. Fossum and G. J. da Silva: Intercalated Water in Synthetic Fluorhectorite Clay. *Langmuir* **26** 9703-9709 (2010).
28. L. E. Michels, H. Hemmen, R. Droppa Junior, G. Grassi, G. J. Silva and J. O. Fossum: Synchrotron X-ray scattering studies of Li-Fluorohectorite synthetic clay: Random intercalation states. *Proceedings of 2nd International Workshop on Complex Physical Phenomena in Materials* (2012).
29. E. DiMasi, J. O. Fossum and G. J. da Silva: *Synchrotron X-ray Study of Hydration Dynamics in the Synthetic Swelling Clay Na-fluorohectorite* Proceedings of the 12th International Clay Conference, Argentina (2003).
30. N. Wada, D. R. Hines and S. P. Ahrenkiel: X-ray diffraction studies of hydration transitions in Na vermiculite. *Phys. Rev. B* **41** 12895-12901 (1990).
31. R. W. Mooney, A. G. Keenan and L. A. Wood: Adsorption of Water Vapor by Montmorillonite. Effect of Exchangeable Ions and Lattice Swelling as Measured by X-Ray Diffraction. *J. Am. Chem. Sot.* **74** 1371-1374 (1952).
32. G. Løvoll, B. Sandnes, Y. Méheust, K. J. Måløy, J. O. Fossum, G. J. da Silva, M. S. P. Mundim, R. Droppa Jr. and D. M. Fonseca: Dynamics of water intercalation fronts in a nano-layered synthetic silicate: A synchrotron X-ray scattering study. *Physica B: Condens. Mat.* **370** 90-98 (2005).
33. G. Strobl, *The Physics of Polymers*, 2nd ed., Springer, p.143-144 (1997).
34. E. Sirota, H. King, D. Singer and H. Shao: Rotator phases of the normal alkanes: An x-ray scattering study. *J. Chem.Phys.* **98** 5809 (1993).
35. G. Ungar: Structure of Rotator Phases in n-Alkanes. *J. Phys. Chem*. **87** 689-695 (1983).
36. M. J. Nowak and S. J. Severtson: Dynamic mechanical spectroscopy of plastic crystalline states in n-alkane systems. *J. Mater. Sci.* **36** 4159–4166 (2001).
37. A. E. Smith: The Crystal Structure of the Normal Paraffin Hydrocarbons. *J. Chem. Phys.* **21** 2229-2231 (1953).

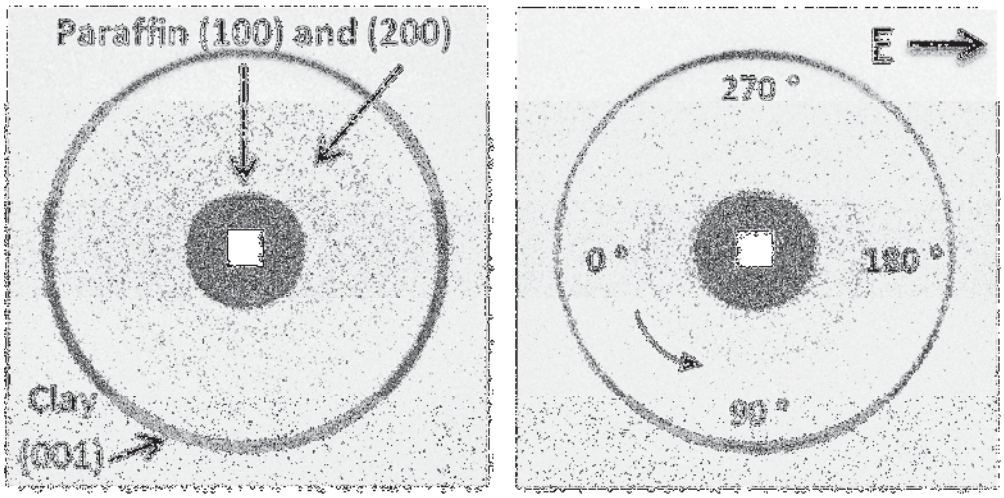

Two-dimensional WAXS patterns from paraffin/clay composites without (left) and with (right) an external E-field of 250 V/mm applied. The outermost ring from clay becomes anisotropic indicating that clay particles are aligned with their stacking direction perpendicular to the E-field lines.

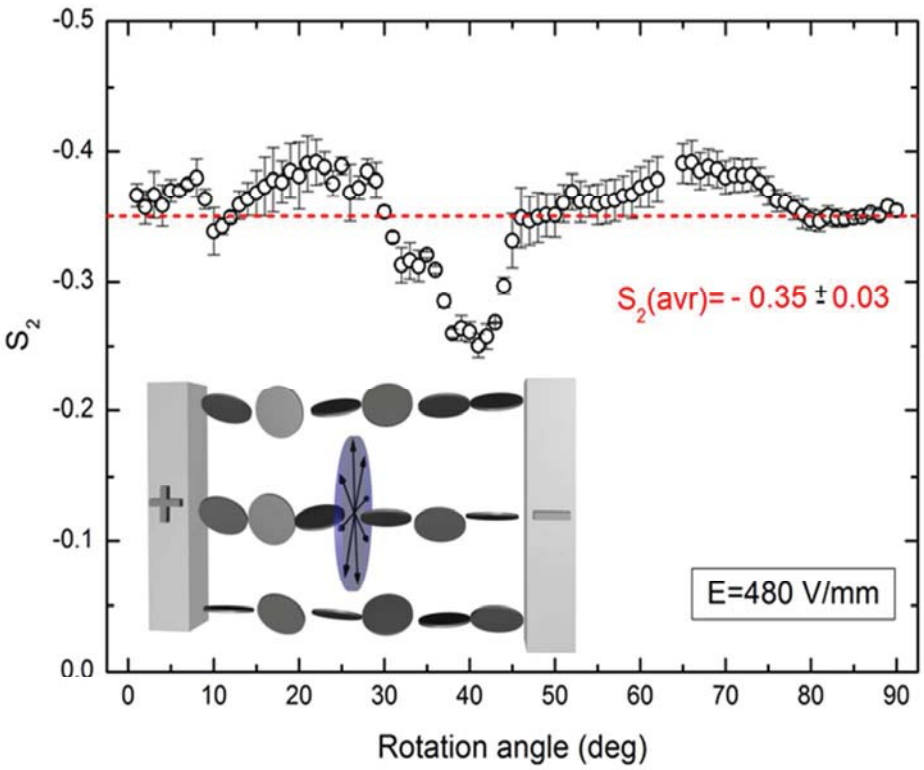

The nematic order parameter calculated for different rotation angles. The average S2 value is indicated as a dashed line. The inset shows a sketch of the clay alignment in a so-called anti-nematic configuration (see text for details).

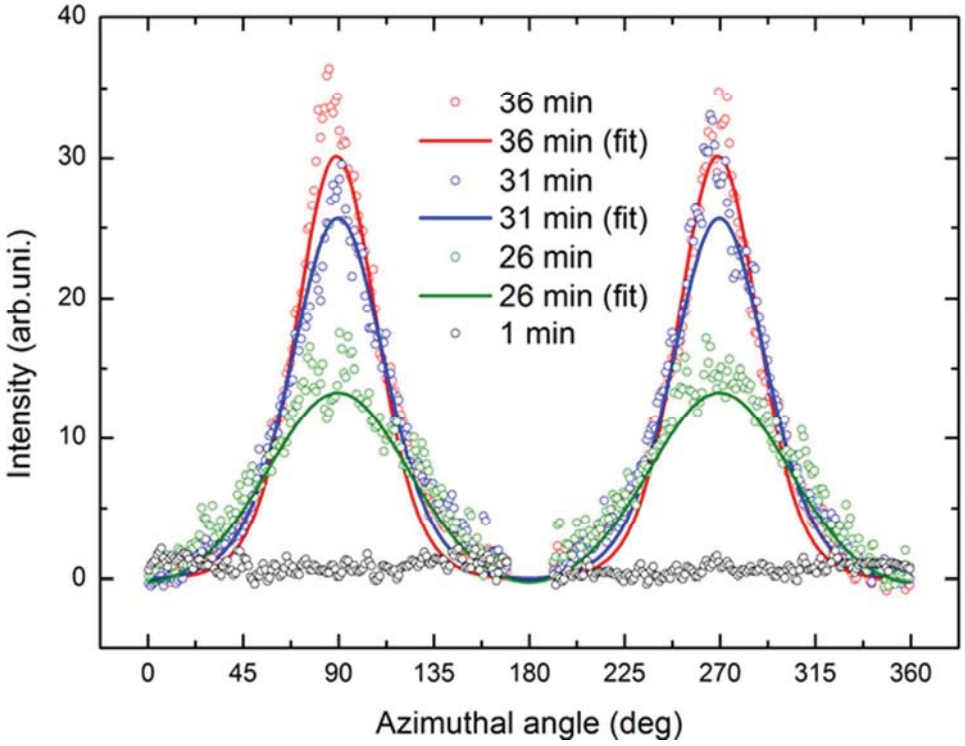

Azimuthal plots of the first Bragg peak amplitude (001) measured at different time during the paraffin melting.

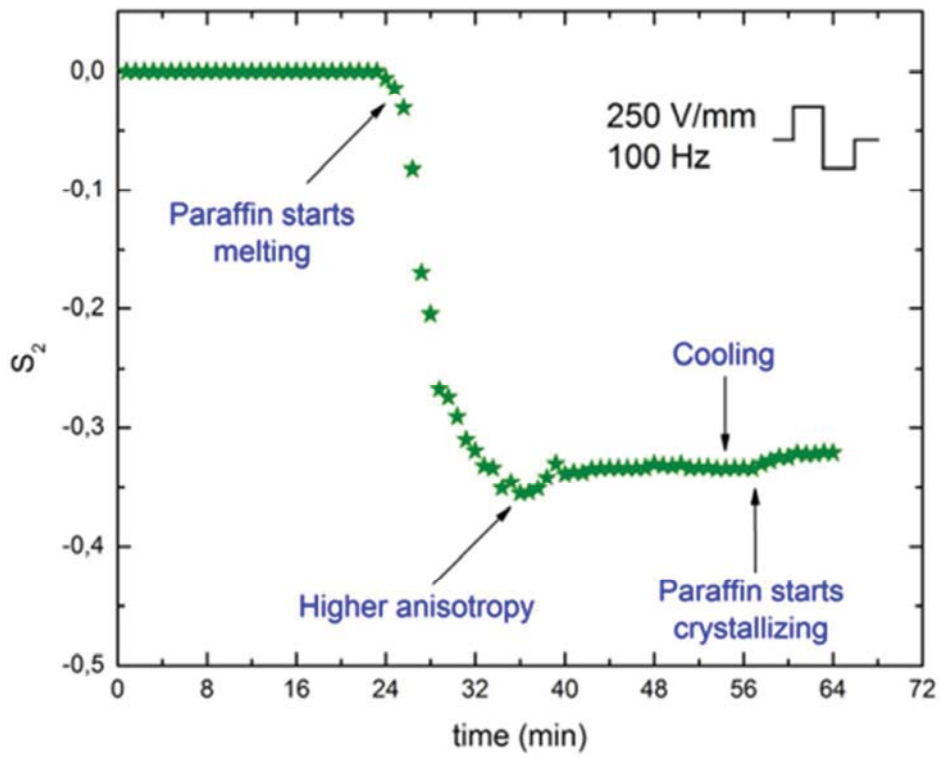

Development of the anisotropy in the system expressed by changes in the nematic order parameter S2.

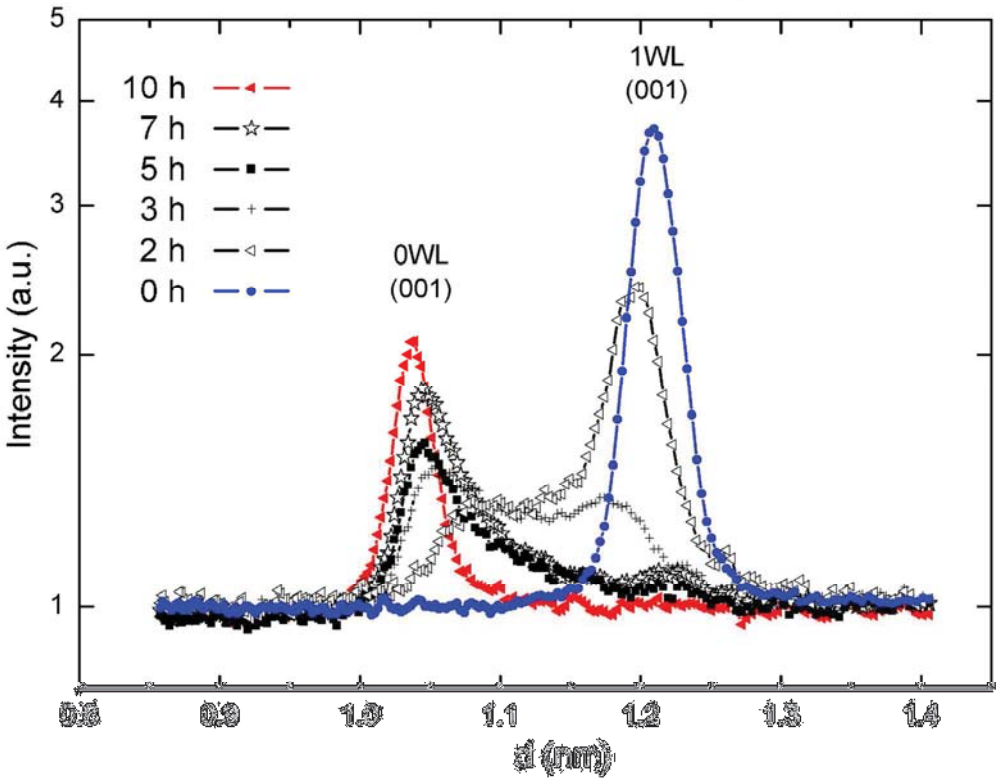

Time evolution of the 1-to-0 water layer transition (Sample batch 2).

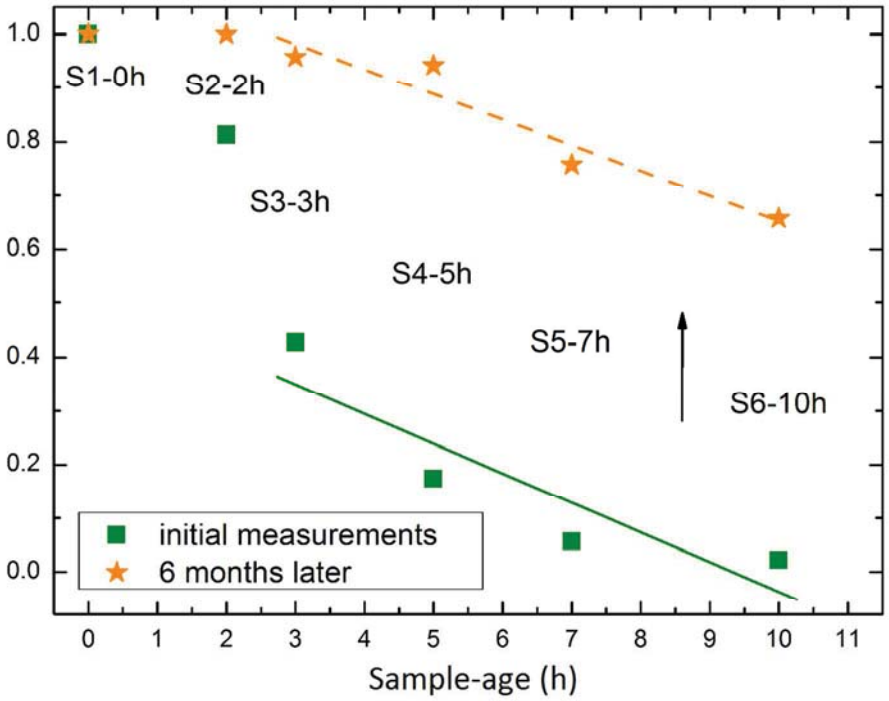

The ratios I1/(I1+ I2) between magnitudes of 0WL and 1 WL peak intensities for 6 samples (Sample batch 2). Their values are in range 0-1, where 0 indicates a pure dehydrated state, 0.5 is obtained when the number of clay particles in the two states are equal, whereas 1 depicts the pure mono-hydrated state.

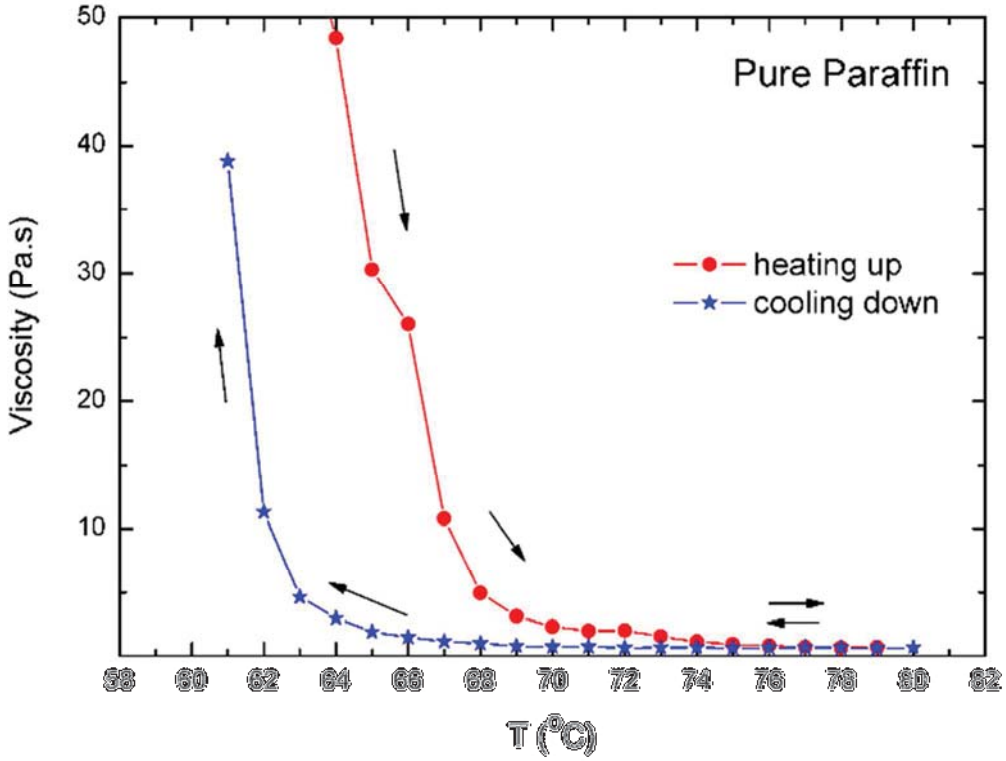

Rheological data showing both the melting and the crystallization transition temperatures for pure paraffin wax used in the present studies, see text.

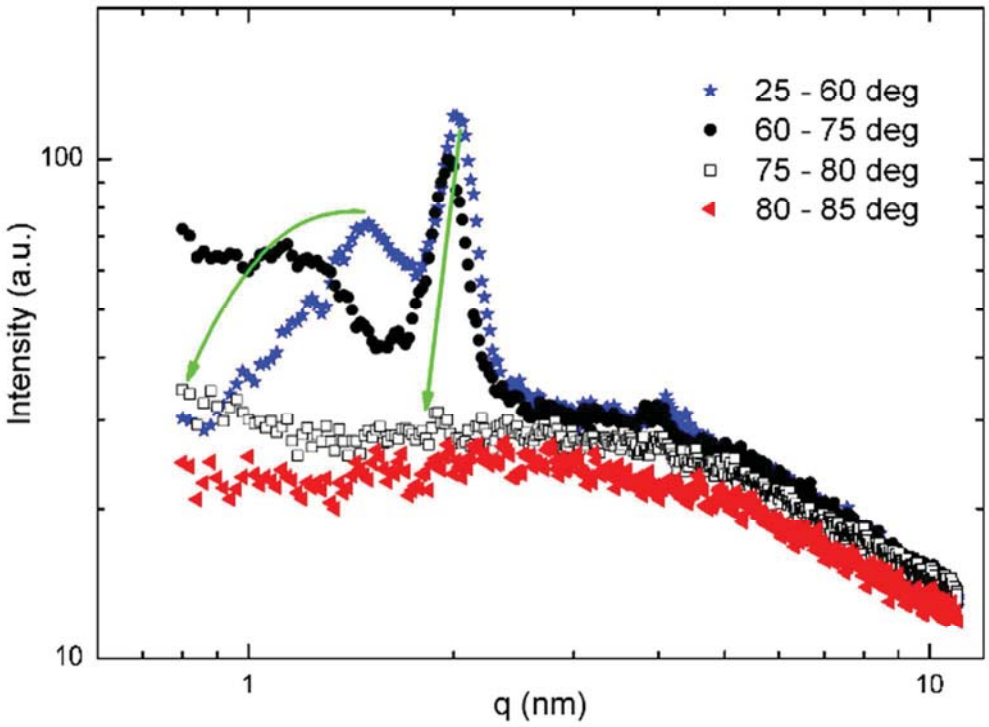

X-ray diffractograms of pure paraffin-wax during heating from 25 to 85 °C. The characteristic peaks attributed to the lengths of the oligomer molecules start shifting and decreasing at temperature range between 60 and 75 °C. They vanish completely for higher temperatures, indicating a loss of crystallinity.

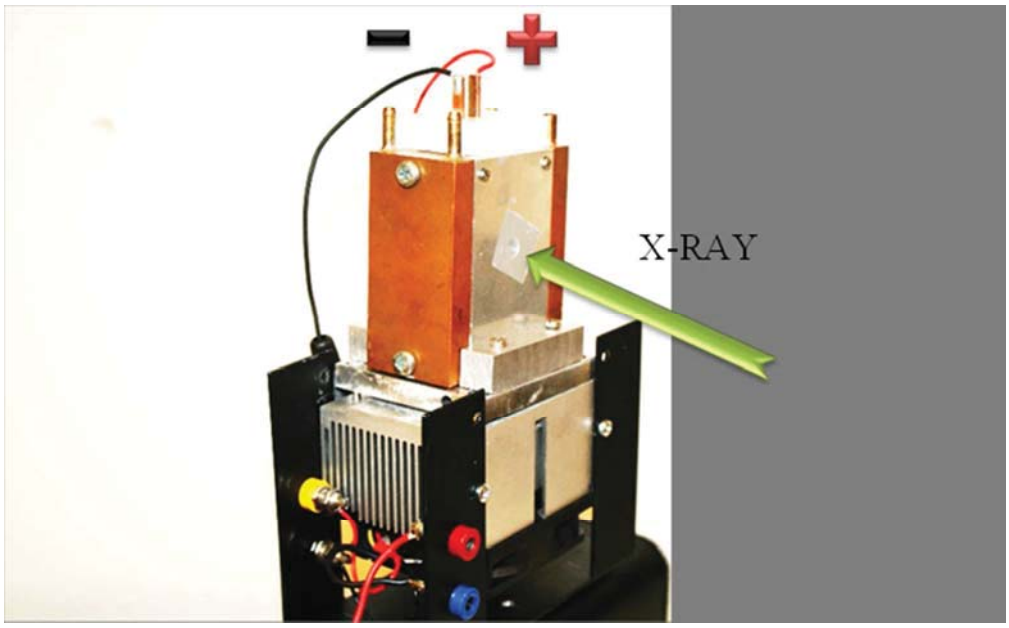

Experimental setup for studying dynamic alignment of clay particles during melting and crystallization of clay/paraffin-wax composites.
225x138mm (72 x 72 DPI)